Environmental Science & Technology

pubs.acs.org/est

Article

Similar Prophage Induction but Divergent Antibiotic Resistance Gene Occurrence: Leachates and Free Radicals Drive Differential Activation Mechanisms in Aged Tire Crumb Rubber

Qiurong Zhang,* Ping Jiang, Chuang Tan, Jie Yu, Wanjun Wang, and Xiang Xiao*

Cite This: *Environ. Sci. Technol.* 2025, 59, 11974−11984

Read Online

ACCESS | Metrics & More | Article Recommendations | Supporting Information

ABSTRACT: Indigenous phages play a key role in the spread of extracellular antibiotic resistance genes (eARGs), and micro/nanocontaminants can exacerbate this process. However, the specific roles and mechanisms of phage communities in this process are still not fully understood. In this study, machine learning models were used to explore how micrometer-sized tire crumb rubber (mTCR) affects the transmission of ARGs via phage communities. The results showed that mTCR at environmentally relevant concentrations significantly activated prophages, promoting the spread of the ARGs. The activation mechanisms of shade- and photoaged mTCR differed, with eARGs carried by phage being more abundant in photoaged mTCR-treated sludge despite similar activation efficiencies. The random forests algorithm revealed that prophage activation induced by shade-aged mTCR was primarily driven by the metals and organic components leached from the mTCR. Antibiotic-resistant lysogens tolerated shade-aged mTCR due to their resistance to metals and organic matter, reducing internal prophage activation. In contrast, photoaged mTCR particles harbored more persistent free radicals, leading to the generation of extracellular $O_2^{\bullet-}$ and $^{\bullet}OH$, which damaged cell membranes and triggered prophage activation. These findings highlight the ecological risk associated with eARGs spread via prophage induction and deepen our understanding of the need to control discarded TCR.

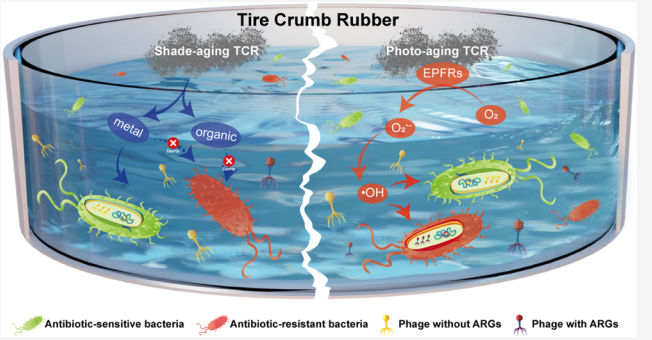

KEYWORDS: *prophage induction, antibiotic resistance genes, tire crumb rubber, leachates, free radicals, environmental aging*

1. INTRODUCTION

The global increase in severe bacterial infections, resulting in nearly 700,000 deaths annually, is directly linked to the rising prevalence of antibiotic resistance genes (ARGs).[1,2] As key vectors of ARGs, phages play a critical role in the development of antibiotic-resistant bacteria.[3−6] Consequently, phage communities in the prevalence of extracellular ARGs (eARGs) raise ecological and health concerns. Within bacterial cells, phages typically undergo the lytic/lysogenic cycle.[7] During the lysogenic stage, phages integrate into the host's genome as prophages and propagate alongside the host's cell division, thus passively spreading ARGs through vertical transfer.[8] When exposed to environmental stressors,[9,10] prophages can be activated to enter the lytic cycle and lead to the production of phages, which facilitates the horizontal transfer of ARGs via phage infection. This lysogenic-lytic switch greatly enhances the development of resistant bacteria by releasing phage particles that carry ARGs.[3,8,11,12] Understanding how environmental factors influence phage community dynamics and the fate of ARGs is crucial for mitigating ARGs transmission and reducing the number of bacterial infections. Preliminary findings find that certain pollutants, such as antibiotics,[9] nanomaterials,[13,14] heavy metals[10] and triclosan,[8] can activate prophages, enhancing the spread of resistance genes. However, how environmental pollutants with varying physicochemical properties alter bacterial metabolic states to trigger the lytic cycle remains unclear. Additionally, the potential impacts of prophage activation on viral community dynamics in natural ecosystems along with the risks of eARGs dissemination have yet to be conclusively established.

Tire crumb rubber (TCR), an emerging contaminant, is discharged into the environment in an estimated 5.92 million tons annually, with a substantial portion entering wastewater system through urban runoff.[15−18] The total microplastic concentrations in sludge are reported to range from 0.4 to 23.5

Received: November 13, 2024
Revised: June 3, 2025
Accepted: June 3, 2025
Published: June 9, 2025

mg/g dry weight,[19] with tire wear particles contributing 30−50% of total microplastic pollution,[20−23] and the concentration of tire wear particles in sludge is estimated to range from 0.12 to 11.75 mg/g dry weight. Wastewater system is a major hotspot for ARGs, where most bacteria harbor prophages that facilitate the spread of resistance genes.[8,12] The substantial introduction of TCR will inevitably cause a negative effect on the transmission of resistance genes. Current studies have reported that the presence of TCR can influence the dissemination of ARGs.[24,25] However, the biological mechanisms by which TCR facilitates the environmental spread of ARGs have not been elucidated. Specifically, it is of great interest to investigate whether TCR affects phage communities in a way that influences the dissemination of ARGs.

Moreover, photoaged micron-sized TCR (mTCR) can generate environmentally persistent free radicals (EPFRs), with the content increasing with photoaging duration.[26,27] Long-term weathering changes the release rate and intensity of toxic substances (e.g., organic compounds and metal ions) from mTCR.[28,29] Theoretically, these changes in the physicochemical properties of mTCR may cause a toxic impact on bacterial metabolism, potentially influencing ARGs spread by phage transduction. However, relevant research in this area is currently insufficient.

This study aims to rigorously assess the exposure risk of TCR in promoting ARG dissemination through phage-mediated pathways and to fully uncover the mechanisms by which environmental aging factors drive this process. For this purpose, we collected TCR debris subjected to natural light/dark aging to evaluate transductive ARGs spread at ambient concentrations.[19] The impact of mTCR on prophage activation and eARGs abundance and diversity was investigated. The contribution of mTCR leachate and its particles to prophage activation was explored in depth using a lysogenic *Escherichia coli* (λ+). Machine learning models (Random Forest) were used to assess the significance of mTCR leachate components on prophage induction. Finally, the different mechanisms resulting in the prevalence of eARGs for dark- and photoaged mTCR were addressed.

2. MATERIALS AND METHODS

2.1. Preparation and Characterization of Tire Rubber Particles. The tire rubber samples were collected from waste tire debris on a high school soccer field in Zhengzhou, Henan Province, China, where they had been aging for three years. We selected two types of tire debris: one that had been fully exposed to sunlight and another that had remained in shaded areas during the three-year period. After collecting the tire debris, we conducted the following pretreatment steps to obtain mTCR for further testing: ultrasonic cleaning with ultrapure water for 15 min, freeze-drying, grinding the samples using a liquid nitrogen ball mill, and sieving through a 200-mesh sieve. The treated black microparticles were designated as "Photoaged mTCR (P-mTCR)" and "Shade-aged mTCR (S-mTCR)", simulating those produced by sunlight exposure, freeze−thaw cycles, and mechanical erosion.[26]

To characterize the leaching of the two tire rubber samples, 1000 mg/L of mTCR particles were immersed in ultrapure water, followed by 30 min of ultrasonication, and shaking at 30 °C for 3 d. The mixture was passed through a 0.22 μm nylon syringe filter, and the resulting filtrate was collected as mTCR leachate. The metals in mTCR leachate were primarily measured for Zn, Fe, As, and Pb, and the organic compounds were quantitatively analyzed for dicyclohexylamine, 4-methylaniline, *N*-cyclohexylformamide, and polycyclic aromatic hydrocarbons (PAHs). The detailed characterization of the mTCR leachate and particles is provided in Sections S1−S3.

2.2. Prophage Activation and eARGs Analysis. *2.2.1. Experiment I: Assessment of Prophage Induction in Sewage Sludge.* Activated sludge samples were collected from the aerobic digestion tanks of three WWTPs located in Zhenjiang, Jiangsu Province; Wuhan, Hubei Province; and Hefei, Anhui Province, China. The samples, designated as ZJ, WH, and HF, respectively, were transported to the laboratory on ice within 4 h. An appropriate amount of wet sludge was mixed with synthetic wastewater (Table S1) and stirred for 30 min. To remove extracellular phages, the sludge was left to settle for 15 min, after which the supernatant was replaced with synthetic wastewater. After being washed three times, appropriate dark-aged or photoaged mTCR was added to the sludge at a concentration of 3.43 mg/g of dry sludge weight. The mixture was incubated in the dark at 37 °C for 4 h.

2.2.2. Experiment II: Phage-like Particle Identification and Quantification. A modified poly(ethylene glycol) (PEG) precipitation method was used to enrich phage-like particles from sludge.[30] Phage-like particles were collected from the supernatant and sludge layer via centrifugation and sonication at 8000 rpm and 4 °C for 5 min, then filtered through 0.45 and 0.22 μm poly(ether sulfone) membranes. The collected filtrate was supplemented with PEG 8000 and NaCl to final concentrations of 10% and 1 M, respectively. After overnight incubation at 4 °C, the mixture was centrifuged at 15,000*g* for 30 min, and the precipitate was resuspended in 2 mL of saline-magnesium buffer for nanoparticle tracking analysis (NTA, Nanosight NS300, Malvern Panalytical, U.K.).[31] Additionally, phage-like particles were stained with uranyl acetate and observed via high-resolution transmission electron microscopy (TEM, JEM-F200, JEOL Ltd., Japan).

2.2.3. Experiment III: Metagenomic Analysis of Bacterial and Viral Profiles. Sewage sludge samples exposed to mTCR for 4 h were collected for metagenomic sequencing on an Illumina HiSeq 2500 instrument (2 × 150 bp, paired-end reads, 10 GB per sample). After quality control with FastQC and Trimmomatic, reads were assembled with MEGAHIT. Prodigal predicted open reading frames, and BWA calculated contig and gene abundance. Species annotation was performed via NCBI-NR using a DIAMOND.

For viral profiles, bacterial cells were removed via centrifugation and filtration. PEG 8000 was added to the filtrate to concentrate the viruses. Phage DNA was extracted with a TaKaRa MiniBEST Kit and sequenced on an Illumina NovaSeq 6000 platform. Sequences ≥ 2000 bp were identified using VirFinder, VirSorter2, and the IMG/VR database. vOTUs were clustered using Mummer with >95% similarity and 85% coverage. VPF-Class was used for species annotation and host prediction. Details are in Sections S4 and S5.

2.2.4. Experiment IV: Prophage-Carried ARGs Identification. Phage sequences were identified using geNomad (v1.6.0), while prophage was predicted with Prophage Hunter (v2.1) with strict cutoff parameters (confidence score >90, att sites confirmed by BLASTN). Only contigs supported by both tools were retained as high-confidence prophage-harboring contigs. Open reading frames (ORFs) within these contigs were extracted, and those located in the predicted prophage regions (defined by Prophage Hunter/geNomad coordinates) were aligned against the SARG database (v3.0) using DIAMOND

https://doi.org/10.1021/acs.est.4c12499
Environ. Sci. Technol. 2025, 59, 11974−11984

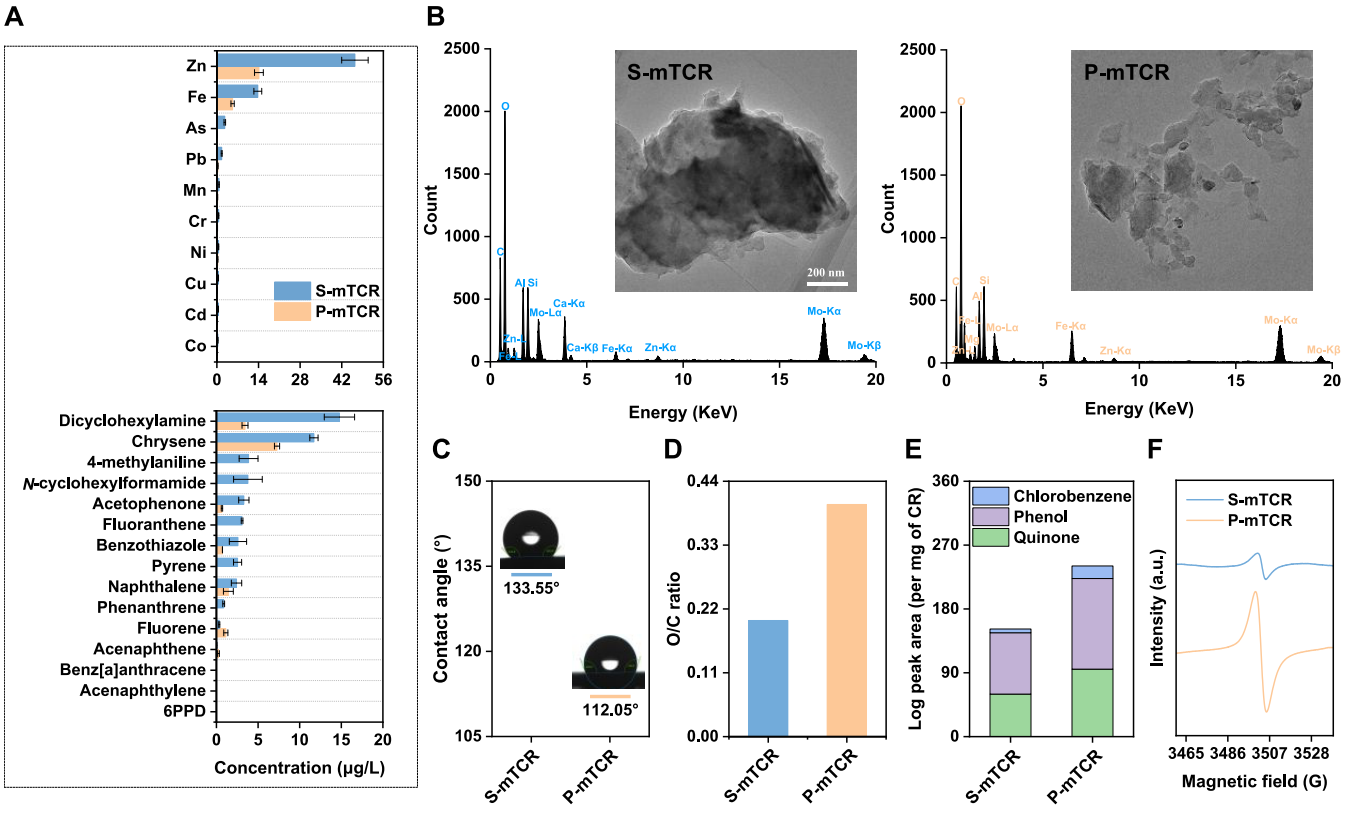

Figure 1. Characterization of dark and photoaged mTCR. (A) Concentration of metals and organic compounds in TCR leachate. (B) Transmission electron microscopy/energy dispersive spectroscopy (TEM/EDS) data for TCR particles. (C) Water contact angle of TCR particles. (D) O/C ratio of TCR particles obtained by XPS analysis. (E) Chlorobenzene, phenol, and quinone-like organic compound content in TCR particles. (F) Persistent free radicals on TCR particles. The results are expressed as the mean value ± SD.

BLASTP with stringent thresholds ($e \leq 1 \times 10^{-5}$, query coverage ≥ 80, and identity ≥ 70%). The detailed process is provided in Section S6.

2.2.5. Experiment V: Virus–Host Interaction Analysis. Virus-host interactions were established using CRISPR spacer, tRNA, homology, and tetranucleotide match methods between viral contigs and metagenome-assembled genomes (MAGs). CRISPR spacers in MAGs were identified with the CRISPR Recognition Tool (CRT). tRNAs were recovered from vOTUs by ARAGORN. The vOTUs were searched against the CRISPR spacer database using blastn short with 97% identity and 90% coverage. tRNA sequences from vOTUs were blasted against MAGs with 100% identity and coverage. Homology matches had an e-value below 10^{-5} and >80% identity over 1 kb and 50% of the host contig. Tetranucleotide frequency analysis compared viral contigs to MAGs for potential host–virus associations.

2.3. Antibiotic Susceptibility and Prophage Activation in Sewage Sludge vs Pharmaceutical Sludge. Pharmaceutical sludge was collected from the aerobic tank of a pharmaceutical manufacturing facilities (PMFs) wastewater treatment plant in Xuzhou, Jiangsu Province, China (Table S2). First, the antibiotic resistance of sewage and pharmaceutical sludges was assessed using disk diffusion and live/dead staining in the presence of antibiotics (ampicillin, gentamicin, and rifampicin) (Section S7). Antibiotic resistance sensitivity of microbial from Zhenjiang WWTP and PMFs was assessed using bioorthogonal noncanonical amino acid tagging (Section S8).[32] Furthermore, the sludge was exposed to the same antibiotics, S-mTCR, and P-mTCR at 3.43 mg/g of dry weight and incubated in the dark at 37 °C for 4 h. Thereafter, phage-like particles were collected and quantified using a Nanosight NS300. Zinc ($ZnCl_2$) and iron ($FeCl_3$) were employed to compare intracellular reactive oxygen species (ROS) levels and prophage activation between antibiotic-sensitive and antibiotic-resistant bacteria (Section S9).

2.4. Contribution of Leachate and Particles to TCR-Induced Phage Activation. *E. coli* DSM4230 without ($\lambda-$) were obtained from DSMZ Braunschweig, Germany. Prophage was established in the $\lambda-$ strain, as detailed in Section S10. Growth experiments were conducted at 37 °C on nutrient broth (NB) medium containing 10.0 g/L tryptone, 3.0 g/L beef extract, 5.0 g/L NaCl, amended with 2.0 g/L maltose, and 0.12 g/L magnesium sulfate heptahydrate. Media were autoclaved at 121 °C, pH 7.2 ± 0.2. TCR leachate, particles, or their mixture were added at 10, 20, 50, 80, and 100 mg/L, corresponding to 0.69, 1.37, 3.43, 5.49, and 6.86 mg/g sludge dry weight. Bacterial suspensions were incubated with TCR at 37 °C for 4 h. Phages were quantified by the two-layer method and NTA measurements. Moreover, intracellular ROS levels and transcriptomic assays of bacteria were assessed. Details are listed in Sections S11–S13.

2.5. Random Forest Feature Importance: Leachate vs Particles Impact. Based on the analysis of metals and organics in TCR leachate, a random forest regression model was constructed using Python's sklearn library. The model included ten variables (Fe, Zn, As, Pb, acetophenone, 4-methylaniline, benzothiazole, *N*-cyclohexylformamide, dicyclohexylamine, and chryzene) as input features and phage activation efficiency as the target variable. Leave-one-out

https://doi.org/10.1021/acs.est.4c12499
Environ. Sci. Technol. 2025, 59, 11974–11984

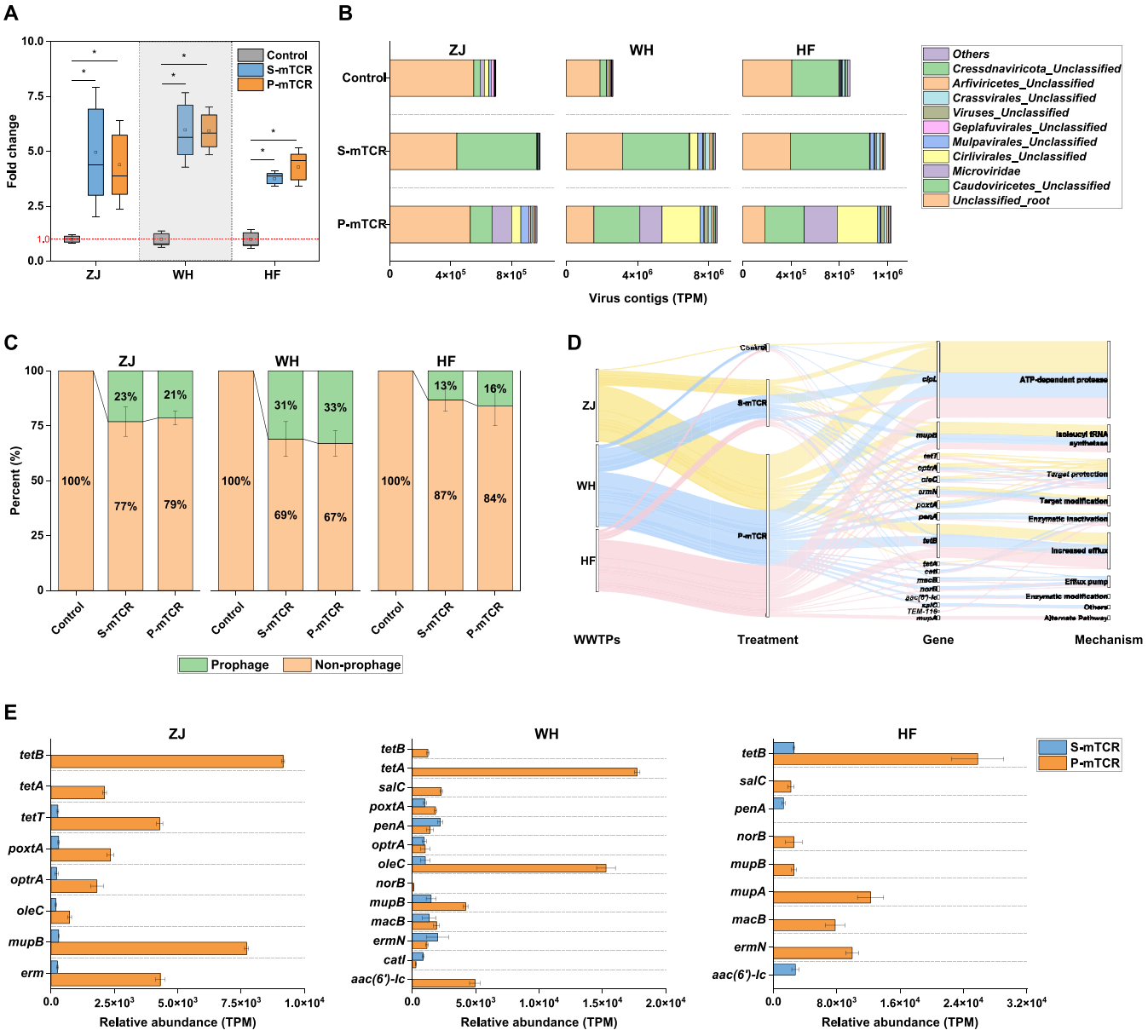

Figure 2. Prophage induction and eARGs changes in WWTP activated sludge. (A) Fold change in phage concentration based on NTA-derived peak distribution of phage-like particles. (B) Viral contigs at the family level. (C) Prophage content change. (D) Sankey diagram linking sample type, phage-carried ARGs, and resistance mechanism. (E) Abundance of prophage-carried ARGs. ZJ, WH, and HF represent Zhenjiang, Wuhan, and Hefei WWTPs, respectively. Sludge treated with 3.43 mg mTCR per gram dry weight for 4 h; untreated sludge as control. The results are expressed as the mean value ± SD; * denotes $p < 0.05$ between the indicated groups.

cross-validation (LOOCV) with mean absolute error (MAE) as the metric was used. Hyperparameters were optimized by using Bayesian algorithms. The best model was cross-validated to determine the feature importance after each training session, ensuring stability. Detailed procedures are in Section S14.

2.6. Oxidative Stress in Different Antibiotic-Resistant Strains with TCR Exposure. Antibiotic-resistant strains used included *E. coli* DH5α carrying plasmid pUC18 (ampicillin resistance, Amp^R), *E. coli* DH5α carrying plasmid pTM (gentamicin resistance, Gm^R), *E. coli* NK5449 (rifampicin resistance, Rif^R), and *E. coli* XL1-blue (tetracycline resistance, Tc^R). These strains were then incubated with a 50 mg/L TCR (dark and photoaged) mixture for 2 h, equivalent to 3.43 mg/g of dry weight of activated sludge. After incubation in the dark for 2 h, bacteria were collected and washed with 0.9% NaCl solution. Intracellular ROS levels were detected using DCFH-DA and visualized with a fluorescence microscope (Axioscope 5, ZEISS, Germany).

2.7. Statistical Analysis. All assays were performed in at least triplicate. For sludge-related experiments, triplicate represents independent experiments, with each sludge sample from different wastewater treatment plants undergoing three technical replicates. Biological replicates were applied in pure culture assays. All the data are expressed as the mean ± SD, and the significance of the differences was determined by an independent *t*-test or one-way ANOVA. A *p*-value less than 0.05 indicated a significant difference.

https://doi.org/10.1021/acs.est.4c12499
Environ. Sci. Technol. 2025, 59, 11974−11984

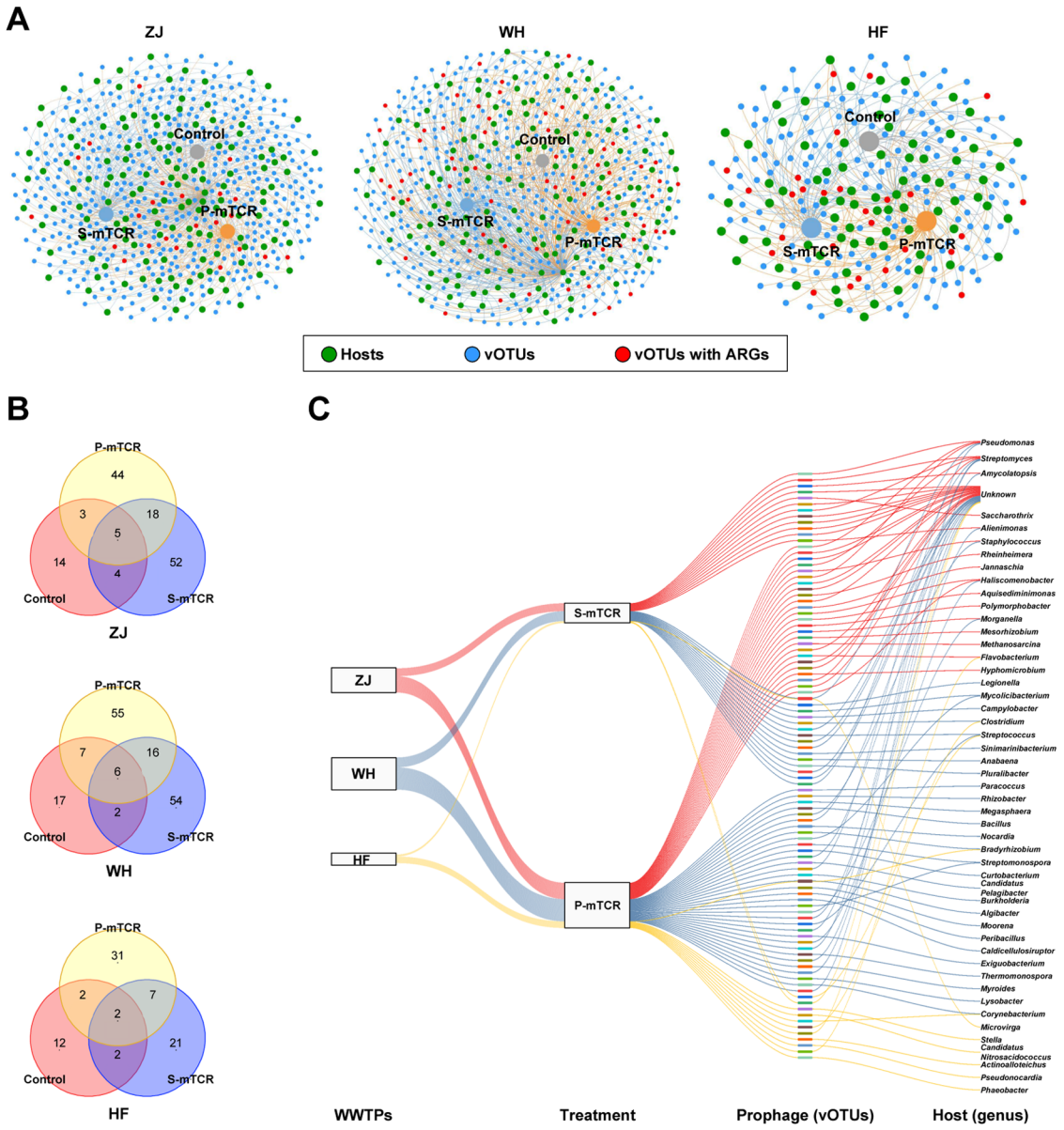

Figure 3. Tracing analysis of activated prophage. (A) Network analysis of prophage-host interactions at the genera level. Green, blue, and red nodes represent host genera, ARGs-free prophages, and ARGs-containing prophages, respectively. (B) Venn diagram of unique and shared hosts at the genera level in control, S-mTCR, and P-mTCR treatments. (C) Prophage-host linkages between ARGs-containing prophages and potential antibiotic-resistant bacteria. ZJ, WH, and HF represent Zhenjiang, Wuhan, and Hefei WWTPs, respectively. Sludge treated with 3.43 mg mTCR per gram dry weight for 4 h; untreated sludge as control.

3. RESULTS AND DISCUSSION

3.1. Alterations in TCR Physicochemical Properties due to Light Exposure. Leachate analysis detected the release of heavy metals (Zn, Fe, As, and Pb, etc.) and organic compounds (dicyclohexylamine, chrysene, 4-methylaniline, *N*-cyclohexylformamide, acetophenone, PAHs, and 6PPD (*N*-(1,3-dimethylbutyl)-*N*′-phenyl-*p*-phenylenediamine)) from TCR (Figure 1A).[33,34] Zn and dicyclohexylamine were the predominant pollutants found in the leachate of S-mTCR. Overall, S-mTCR leachate had higher metal and organic concentrations than P-mTCR leachate, contradicting reports that photoaging accelerates the release of these pollutants from tire wear particles (Figure 1A).[28,29] This difference may arise because laboratory light aging of tire wear particles typically only lasts about a month and lacks exposure to environmental factors such as rainwater flushing and weather changes.[27,28,35] In this study, by contrast, P-mTCR from natural environments underwent prolonged aging (about three years) and faced various weather conditions such as rainfall and freeze−thaw cycles, which may result in the massive loss of heavy metals and organic pollutants.

S-mTCR displayed a dense and relatively uniform structure with large, aggregated flakes, while P-mTCR showed smaller fragmented flakes with less distinct edges, suggesting more advanced weathering (Figure 1B). This weathering increased P-mTCR's dispersibility in water by enhancing its hydrophilicity and introducing more oxygen-containing functional groups on its surface (Figures 1C,D and S1). Energy dispersive X-ray spectroscopy revealed that both shade-aged and photoaged TCR contained a variety of metal elements, including Zn, Mg, Al, Si, Mo, Cu, and Fe (Figure 1B),

https://doi.org/10.1021/acs.est.4c12499
Environ. Sci. Technol. 2025, 59, 11974−11984

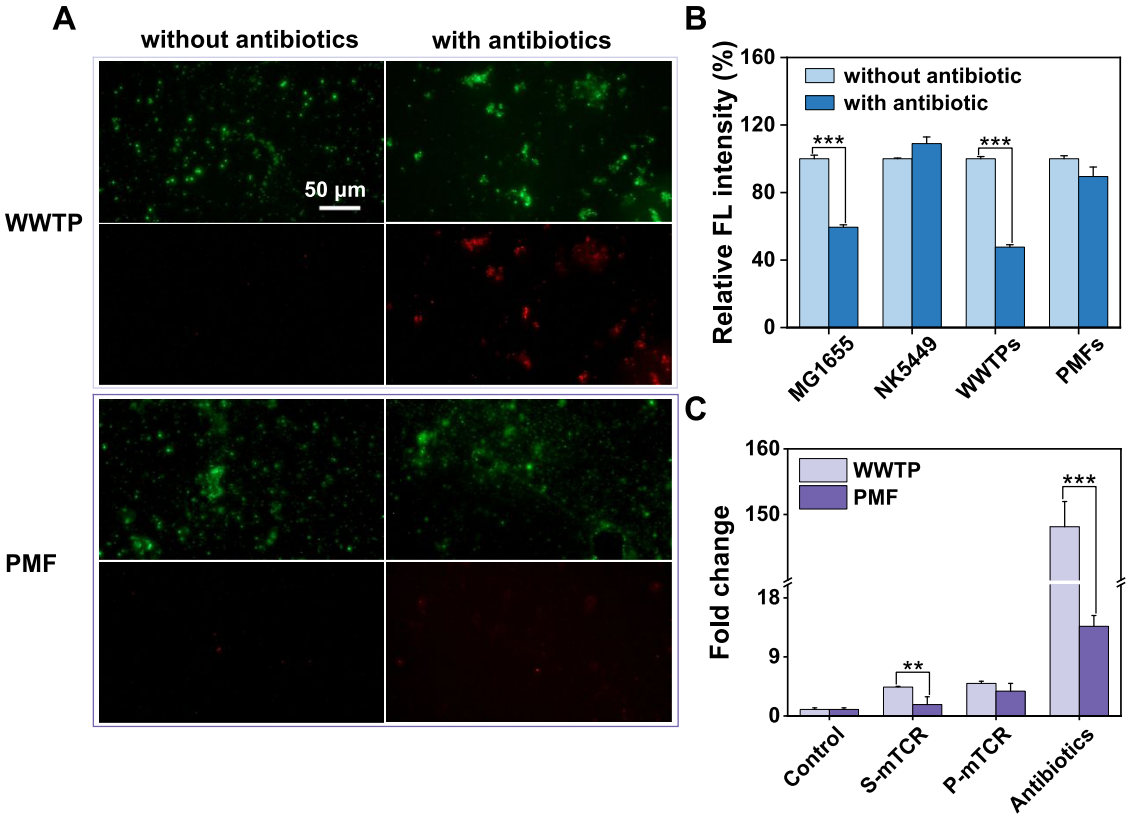

Figure 4. Differences in prophage activation in Zhenjiang WWTP and PMF sludge after TCR exposure. (A) Live/dead staining. (B) Fluorescence intensity of homopropargylglycine-labeled bacteria. (C) Fold change in phage concentration. Sludge treated with 3.43 mg mTCR per gram for 4 h. Untreated sludges as controls. The results are expressed as the mean value ± SD; ** and *** represent $p < 0.01$ and $p < 0.001$, respectively.

aligning with previous studies.[36] Moreover, P-mTCR shows higher levels of chlorobenzene, phenol, and quinone compared to S-mTCR (Figure 1E), correlating with their higher EPFR concentrations (Figure 1F). EPFR levels have increased from 1.3×10^{16} spins/g in S-mTCR to 1.2×10^{17} spins/g in P-mTCR. These types of compounds (e.g., pentachlorophenol,[37] 1,2-dichlorobenzene,[38] 2,6-dibromohydroquinone,[39] and phenol[40]) contributed to the formation of persistent free radicals (Figure S2). In summary, P-mTCR exhibited a higher degree of aging compared to S-mTCR (Figure 1B−1F), indicating that P-mTCR had released metals and organic matter earlier. Thus, moderately aged S-mTCR retained a higher ability to release metals and organic matter compared with P-mTCR (Figure 1A). This result demonstrated that aging conditions and collection time of aged samples significantly impact pollutant release from rubber particles.

3.2. Varied eARGs Abundance Despite Similar Prophage Induction: Dark vs Photoaged TCR. NTA measurements showed that S-mTCR and P-mTCR significantly increased prophage activation in sludge from all three WWTPs (ZJ, WH, and HF), with the highest fold changes in sludge from Wuhan WWTP reaching 5.97 and 5.93, respectively (Figures 2A and S3). TEM imaging, using sludge from Zhenjiang WWTP as an example, further confirmed the presence of various phage-like particles in the activated sludge (Figure S4).[41] Under specific triggers like DNA damage or environmental stress, prophages can shift from lysogenic to lytic states, releasing phage particles into the environment.[7] These phages infect other bacteria and start new lysis cycles,[7] which changes the proportions and distributions of phages and their carried ARGs.[42] Viral metagenomic sequencing revealed that mTCR exposure led to significant changes in phage communities (Figure 2B). This occurred despite the microbial community structure remaining relatively stable (Figure S5). Notably, viral contigs annotated as prophages were scarcely detected in the control group (Figure 2C). In contrast, S-mTCR and P-mTCR treatment significantly increased the proportion of prophages in the activated sludge from all three WWTPs, rising from nearly 0 to 13−33%. This indicates that mTCR exposure triggered prophage activation, causing cell lysis and the release of bacterial genomic DNA in the activated sludge.

Naturally, prophages often carry ARGs, which are released into the extracellular environment during bacterial cell lysis.[3] The monkey diagram illustrates the linkage between WWTPs, treatments, ARGs-carrying prophages, and resistance mechanisms (Figure 2D). Major resistance pathways, particularly efflux pumps (e.g., *tet* genes) and target modification (e.g., *erm* genes), demonstrated stronger association with P-mTCR treatment compared to S-mTCR treatment. The genes *tetA*, *tetB*, and *tetT* confer resistance to tigecycline, tetracycline, and doxycycline, respectively.[43] *poxtA* grants resistance to chloramphenicol, florfenicol, linezolid, doxycycline, and tetracycline.[44,45] *mupB* and *mupA* enable resistance to mupirocin.[46] *erm* is linked to resistance to erythromycin, lincomycin, clindamycin, quinupristin, pristinamycin IA, and virginiamycin *S. ole* confers resistance to oleandomycin, and *optrA* provides resistance to linezolid, chloramphenicol, and florfenicol (Figure 2D).[47] Strikingly, the relative abundance of activated prophages carrying ARGs in all activated sludge samples from all three WWTPs (ZJ, WH, and HF) was significantly higher in the P-mTCR treatment compared to the S-mTCR

https://doi.org/10.1021/acs.est.4c12499
Environ. Sci. Technol. 2025, 59, 11974−11984

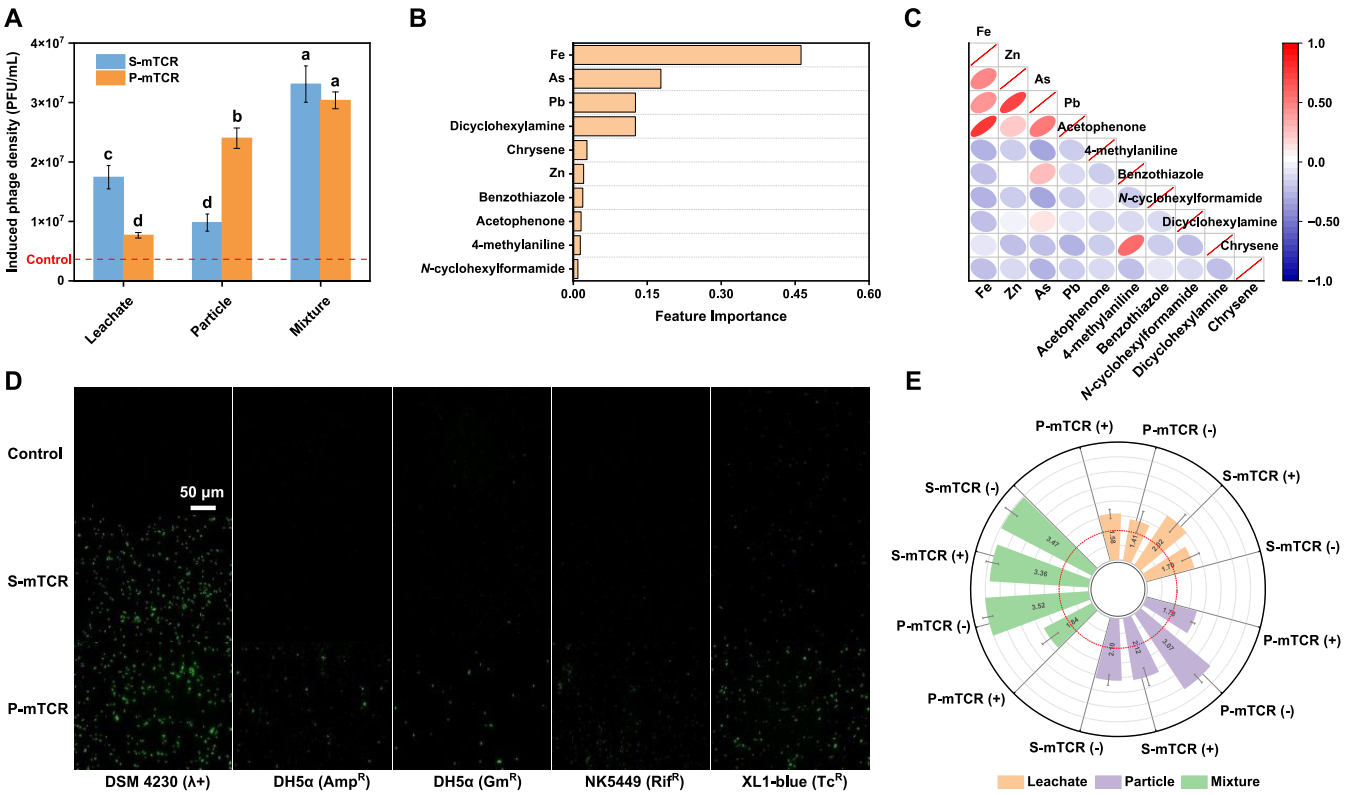

Figure 5. Effects of leachate and particles on mTCR-induced prophage activation. (A) Prophage quantification. (B) Feature importance of metals and compounds in prophage induction. (C) Correlation matrix of metals and organic compounds on prophage activation. (D) Intracellular ROS response. (E) Impact of $O_2^{\bullet-}$ scavenger on prophage activation. *E. coli* (λ+) was treated with 50 mg/L mTCR fractions for 4 h; untreated group as control. The results are expressed as the mean value ± SD. Different letters denote $p < 0.05$.

group (Figure 2E). This result indicates that both dark-aged and photoaged CR induce prophage activation and alert phage communities. Notably, although two types of mTCR exhibit similar efficiencies in inducing prophage activation (Figure 2A–2C), photoaged mTCR-treated activated sludge from all three WWTPs (ZJ, WH, and HF) shows a higher prevalence of eARGs compared to dark-aged mTCR-treated sludge.

3.3. Insignificant Impact of Dark-Aged TCR on Prophage Activation in Antibiotic-Resistant Bacteria. The activation of prophages by environmental stress (e.g., antibiotics, metal ions) is linked to the interaction between prophages and their hosts, as these pollutants can induce bacterial stress responses like DNA damage and SOS system.[12] As shown in Figure 3A, the prophage-host networks for each WWTP (ZJ, WH, and HF) revealed that both S-mTCR and P-mTCR treatments increased the complexity of prophage–host interactions, particularly those involving ARGs-carrying prophages (red nodes). The number of host genera associated with prophages was substantially higher in the S-mTCR and P-mTCR groups compared to the control across all three WWTPs (Figure 3B). For instance, in the ZJ sample, 52 and 44 unique host genera were identified under S-mTCR and P-mTCR treatments, respectively, while only 14 were found in the control. Notably, only 23, 22, and 9 genera were commonly observed in both mTCR treatments in ZJ, WH, and HF, respectively (Figure 3B), suggesting that S-mTCR and P-mTCR induced prophage activation through different mechanisms, likely driven by their distinct aging processes and chemical properties. While the overall numbers of activated prophages were similar in both mTCR treatments (Figure 2A), the host association patterns of ARGs-containing prophages exhibited marked differences (Figure 3C). Given that ARGs are initially randomly integrated into the bacterial genome, variations in their presence within prophages may reflect differences in the extent of ARGs dissemination among different genera. For example, *Pseudomonas aeruginosa*, a common pathogen with resistance to multiple antibiotics in hospital infections,[48] was detected as the most vOTUs with ARGs in all identified genera (Figure 3C).

Considering the limited overlap in host genera across different mTCR treatments, we hypothesize that S-mTCR and P-mTCR may induce prophage activation through distinct mechanisms. Furthermore, with a lower proportion of ARGs-containing prophages in the S-mTCR treatment than in the P-mTCR treatment, prophage activation was compared in antibiotic-resistant sludge from PMFs and antibiotic-sensitive sludge from WWTPs under mTCR exposure. Results showed that under exposure to antibiotics, the mortality of bacteria in activated sludge from WWTPs was higher than that in sludge from PMFs (Figure 4A). Metabolism activity assay using bioorthogonal noncanonical amino acid tagging showed that antibiotics significantly hindered protein synthesis in the sensitive strain MG1655 and microbial communities from WWTPs sludge, indicating that activated sludge from WWTPs was more sensitive to antibiotics than PMFs sludge (Figure 4B). Moreover, prophage activation in S-mTCR treatments also varied, showing a more pronounced decrease in antibiotic-resistant sludge from PMFs compared with the more antibiotic-sensitive sludge from WWTPs, similar to the effects seen under antibiotic treatment (Figure 4C). In contrast, no significant change in prophage activation was observed between sludge communities from PMFs and WWTPs under

https://doi.org/10.1021/acs.est.4c12499
Environ. Sci. Technol. 2025, 59, 11974–11984

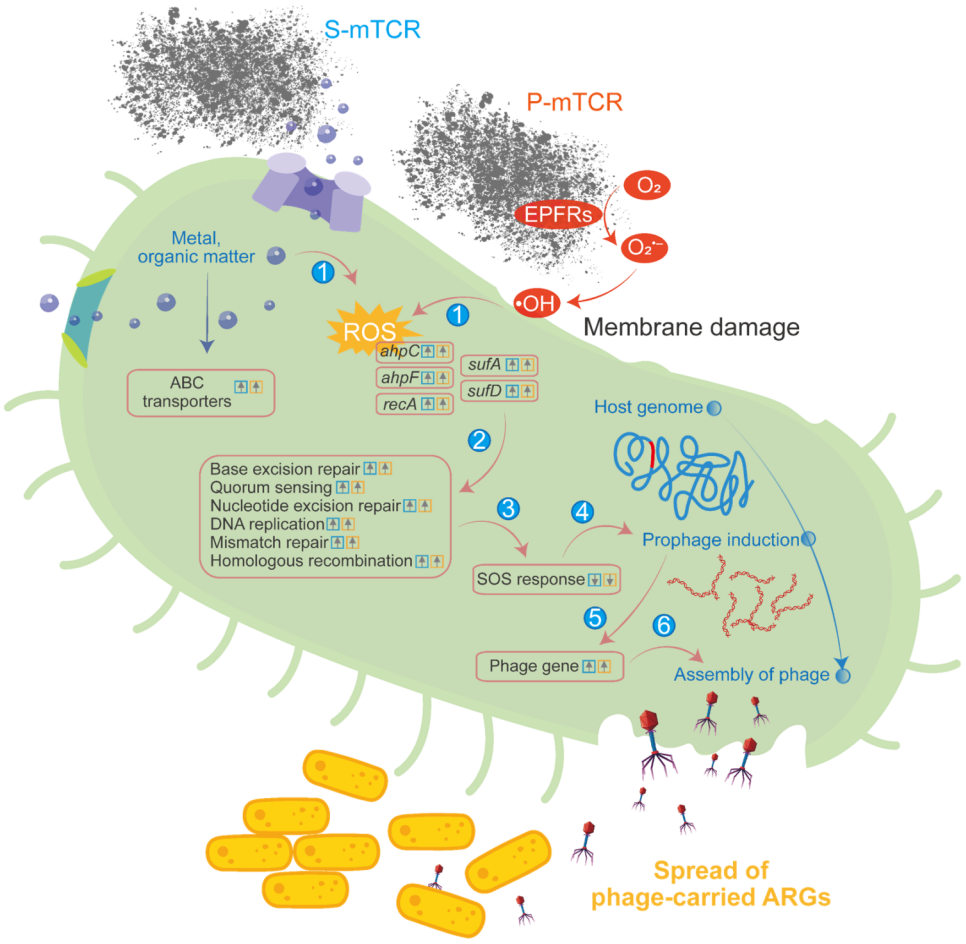

Figure 6. Proposed mechanisms of mTCR triggering prophage induction and promoting the transduction of released ARGs-containing prophages. Differentially expressed genes in transcriptomics relevant to λ phage activation in *E. coli* (λ+). *E. coli* (λ+) was treated with 50 mg/L mTCR fractions. Untreated group was used as control.

P-mTCR treatment (Figure 4C). This indicated that antibiotic-resistant lysogens may be tolerant to S-mTCR, thereby mitigating the activation of internal prophages. Common resistance mechanisms in prokaryotes against antibiotics and metals[49] (or organic matter)[50] are frequently observed. The distinct mechanisms of S-mTCR and P-mTCR on antibiotic-resistant lysogens may arise from the differing roles of the mTCR physicochemical properties in prophage activation.

3.4. Key Physicochemical Properties of mTCR in Prophage Activation. To further determine the mechanism of mTCR on prophage activation, an *E. coli* (λ+) strain was used to analyze the key physicochemical properties of mTCR that trigger prophage induction. Despite similar activation efficiencies being observed in the mixture treatments of S-mTCR and P-mTCR, S-mTCR leachate induced more prophage activation than P-mTCR leachate. Conversely, P-mTCR particles were more effective than S-mTCR particles in activating prophages (Figures 5A and S6). Based on an analysis of metals and organics in TCR leachate, a comprehensive random forest regression model was developed, and an R-squared value of 0.85 was achieved (Section S14), indicating strong explanatory power. The feature importance analysis of various metals and organics in mTCR-induced prophage activation revealed that Fe had the highest contribution to prophage activation (score ∼0.46), followed by As and Pb (scores 0.18−0.13) (Figure 5B). In contrast, organics were significantly less important. Apart from dicyclohexylamine, the feature importance scores for other organics were below 0.03. Figure 5C presents a correlation matrix of different metals and organics involved in mTCR-induced prophage activation. The colors represent the strength and direction of the correlations (positive or negative). Leachate components showed synergistic effects, notably between metals (Figure 5C). These results indicated that leachate, especially its metal fractions, contributed to S-mTCR-induced prophage activation.

Metals and organic pollutants act as inducers to promote phage activation due to their toxicity to microorganisms.[20,51−53] However, antibiotic-resistant strains often show co- or cross-resistance to metals by reducing permeability, altering drugs/metals, enhancing efflux, modifying targets, or sequestering substances.[49] Additionally, PAHs can also affect bacterial efflux pumps, inducing mutations that enable resistance to both antibiotics and PAHs.[50] As shown in Figure 5D, for the antibiotic-sensitive strain DSM4230(λ+), both S-mTCR and P-mTCR treatments increased intracellular oxidative stress with no significant difference between them. However, in strains with different antibiotic resistance phenotypes, S-mTCR treatment did not induce intracellular ROS generation, whereas P-mTCR treatment still triggered oxidative stress. These results showed that S-mTCR failed to induce oxidative stress toxicity in antibiotic-resistant bacteria, aligning with the observed decrease in prophage activation in

https://doi.org/10.1021/acs.est.4c12499
Environ. Sci. Technol. 2025, 59, 11974−11984

antibiotic-resistant sludge from PMFs compared to more antibiotic-sensitive sludge from WWTPs (Figure 4C). Additional experiments involving zinc and iron demonstrated that antibiotic-resistant bacteria are also resistant to heavy metals. Treatment with 10−50 mg/L $ZnCl_2$ or 50 mg/L $FeCl_3$ significantly increased intracellular ROS levels in WWTPs sludge, whereas no notable effect was observed in PMFs sludge (Figure S7A,B). Furthermore, phage concentrations in WWTPs sludge were elevated following treatment with 20 mg/L $ZnCl_2$ or 50 mg/L $FeCl_3$, while no significant differences were observed in PMFs sludge (Figure S7C). This suggests that co- or cross-resistance between antibiotic and metal allows antibiotic-resistant lysogens to tolerate S-mTCR, leading to a lower release of ARGs-containing prophages.

For S-mTCR, intracellular ROS increased in *E. coli* DSM 4230 (λ+), but outer membrane permeability did not change (Figure S8). However, P-mTCR exposure increased both intracellular ROS and the outer membrane permeability in lysogenic bacteria. High levels of persistent free radicals were detected on P-mTCR particles (Figure 1F), leading to elevated levels of extracellular $O_2^{\bullet-}$ (Figure S9A). These unstable extracellular $O_2^{\bullet-}$ quickly transformed into extracellular $^{\bullet}OH$ (Figure S9B), disrupting outer membrane stability.[14] The presence of $O_2^{\bullet-}$ scavenger thiourea significantly inhibited λ phage activation induced by P-mTCR but barely impact the prophage activation in the S-mTCR group (Figure 5E). Thus, persistent free radicals on P-mTCR particles induced the production of extracellular $O_2^{\bullet-}$ and $^{\bullet}OH$, which impaired the outer membrane and then indirectly triggered intracellular oxidative stress.

Elevated intracellular ROS can lead to DNA damage.[54] After exposure to mTCR, *E. coli* (λ+) upregulated genes related to DNA repair pathways (Figures 6 and S10). For example, SOS response-associated genes, e.g., *recA*, *umuC*, *sulA*, *dinB*, and *ruvA*, all increased over 1.6-fold after treated by mTCR (Figure S11). To mitigate the oxidative stress, the expression of genes related to the oxidative stress system (e.g., *ahpC, ahpF, sufA,* and *sufD*) was upregulated. Especially importantly, genes linked to λ phage replication and assembly also increased significantly when exposed to both dark- and photoaged mTCR (Figure 6), indicating the improvement of prophage induction. Therefore, whether directly via leachate or indirectly via persistent free radicals, S-mTCR and P-mTCR induced intracellular ROS, leading to DNA damage, activating the SOS response, and ultimately triggering prophage activation and release. Our findings reveal how S-mTCR and P-mTCR facilitate the spread of ARGs by triggering prophage activation through distinct mechanisms.

4. ENVIRONMENTAL IMPLICATIONS

With annual global emissions of 5.92 million tons, the persistence of TCR has led to a gradual environmental concentrations, which inevitably spread across various environmental scenarios.[35] As major reservoirs for TCR, WWTPs have accumulated significant amounts of TCR, with sludge concentrations reaching up to 42.7 g/kg.[15] Additionally, indigenous lysogenic bacteria harboring prophages are highly abundant and diverse in WWTPs.[12] Such a spatial coexistence provides opportunities for intensive TCR-lysogen interactions. Consequently, TCR particles and their leachate will trigger the activation of prophages, resulting in the disintegration of lysogenic cells and the release of newly formed phages. These eARGs may transfer to other bacteria through transformation and transduction, leading to the spread of eARGs among the bacterial populations. Moreover, the physicochemical properties of RCE will be altered when exposed to real environmental conditions. Variations in the adsorption capacity, surface activity, and reactivity of aged TCR can affect the efficiency and mechanisms underlying prophage activation, resulting in substantial environmental consequences and ecological risks.

Overall, this study uniquely demonstrated that TCR exposure contributed to improving the ARGs dissemination by phage transduction. While both shaded and photoaged mTCR induced similar shifts in phage communities within activated sludge, they exhibited distinct impacts on the spread of extracellular eARGs. Further analysis revealed that shade-mTCR activated prophages primarily through metals and organics in leachate, whereas persistent free radicals generated by photoaged mTCR were more effective at prophage activation in antibiotic-resistant lysogens. Our findings provide new insights into the environmental risks associated with discarded TCR and deepen our understanding of eARGs dissemination caused by prophage activation.

■ ASSOCIATED CONTENT

Supporting Information

The Supporting Information is available free of charge at https://pubs.acs.org/doi/10.1021/acs.est.4c12499.

Additional method details (Supporting Methods); composition of synthetic wastewater (Table S1); characteristics of sewage and pharmaceutical sludges (Table S2); instrumental parameters used in LC-HRMS (Table S3); primers used in the qRT-PCR (Table S4); XPS spectra of the C 1s peaks of dark and photoaged mTCR particles (Figure S1); EPFR formation from hydroquinone, phenol, pentachlorophenol, and 1,2-dichlorobenzene involves transition metal interactions (Figure S2); Phage-like particle concentration and size distributions by NTA (Figure S3); TEM image of phage in activated sludge from Zhenjiang WWTP (Figure S4); species distribution at phylum classification level for samples after mTCR treatment (Figure S5); quantification and morphological analysis of λ phage activated from *E. coli* (λ+) (Figure S6); differences in prophage activation in Zhenjiang WWTP and PMFs sludge after metal ion exposure (Figure S7); effects of shade- and photoaged mTCR on ROS and membrane permeability (Figure S8); EPR analysis of extracellular $O_2^{\bullet-}$ and $^{\bullet}OH$ on mTCR particles (Figure S9); enrichment analysis identified upregulated gene terms after mTCR treatment (Figure S10); and changes in gene expression related to the SOS response over treatment time (Figure S11) (PDF)

■ AUTHOR INFORMATION

Corresponding Authors

Qiurong Zhang − *Information Materials and Intelligent Sensing Laboratory of Anhui Province, Institutes of Physical Science and Information Technology, Anhui University, Hefei 230601, China;* orcid.org/0000-0002-3045-7197; Email: zhangqiurong@ahu.edu.cn

Xiang Xiao − *Information Materials and Intelligent Sensing Laboratory of Anhui Province, Institutes of Physical Science and Information Technology, Anhui University, Hefei*

230601, China; orcid.org/0000-0002-3987-8668; Email: xiaox@ustc.edu.cn

Authors

Ping Jiang − *Information Materials and Intelligent Sensing Laboratory of Anhui Province, Institutes of Physical Science and Information Technology, Anhui University, Hefei 230601, China;* orcid.org/0009-0008-4522-2586

Chuang Tan − *Information Materials and Intelligent Sensing Laboratory of Anhui Province, Institutes of Physical Science and Information Technology, Anhui University, Hefei 230601, China;* orcid.org/0009-0003-4120-2741

Jie Yu − *Information Materials and Intelligent Sensing Laboratory of Anhui Province, Institutes of Physical Science and Information Technology, Anhui University, Hefei 230601, China;* orcid.org/0009-0005-6590-0987

Wanjun Wang − *Institute of Environmental Health and Pollution Control, Guangdong University of Technology, Guangzhou 510006, China;* orcid.org/0000-0003-1193-1030

Complete contact information is available at: https://pubs.acs.org/10.1021/acs.est.4c12499

Notes

The authors declare no competing financial interest.

■ ACKNOWLEDGMENTS

This work was partially supported by the National Natural Science Foundation of China (52170015, 22106004, and 52470171) and the University Synergy Innovation Program of Anhui Province (GXXT-2021-040).

■ REFERENCES

(1) Ko, K. K. K.; Chng, K. R.; Nagarajan, N. Metagenomics-enabled microbial surveillance. *Nat. Microbiol.* **2022**, *7*, 486−496.

(2) Uyttebroek, S.; Chen, B.; Onsea, J.; Ruythooren, F.; Debaveye, Y.; Devolder, D.; Spriet, I.; Depypere, M.; Wagemans, J.; Lavigne, R.; Pirnay, J. P.; Merabishvili, M.; De Munter, P.; Peetermans, W. E.; Dupont, L.; Van Gerven, L.; Metsemakers, W. J. Safety and efficacy of phage therapy in difficult-to-treat infections: A systematic review. *Lancet Infect. Dis.* **2022**, *22*, e208−e220.

(3) Liu, W.; Xu, C.; Li, T.; Ren, Z.; Hao, S.; Chen, Z.; Huang, X.; Wen, X. Temporal dynamics and contribution of phage community to the prevalence of antibiotic resistance genes in a full-scale sludge anaerobic digestion plant. *Environ. Sci. Technol.* **2024**, *58*, 6296−6304.

(4) Pfeifer, E.; Bonnin, R. A.; Rocha, E. P. C. Phage-plasmids spread antibiotic resistance genes through infection and lysogenic conversion. *mBio* **2022**, *13*, No. e0185122.

(5) Li, Z.; Guo, X.; Liu, B.; Huang, T.; Liu, R.; Liu, X. Metagenome sequencing reveals shifts in phage-associated antibiotic resistance genes from influent to effluent in wastewater treatment plants. *Water Res.* **2024**, *253*, No. 121289.

(6) Zhang, P.; Wang, Y.; Lin, H.; Liang, J.; Wang, J.; Bai, Y.; Qu, J.; Wang, A. Bacterial evolution in biofiltration of drinking water treatment plant: Different response of phage and plasmid to varied water sources. *Water Res.* **2024**, *259*, No. 121887.

(7) Chevallereau, A.; Pons, B. J.; van Houte, S.; Westra, E. R. Interactions between bacterial and phage communities in natural environments. *Nat. Rev. Microbiol.* **2022**, *20*, 49−62.

(8) Lu, J.; Guo, J. Prophage induction by non-antibiotic compounds promotes transformation of released antibiotic resistance genes from cell lysis. *Water Res.* **2024**, *263*, No. 122200.

(9) Zhang, Y.; Liao, Y.; Salvador, A.; Sun, X.; Wu, V. C. H. Prediction, diversity, and genomic analysis of temperate phages induced from Shiga toxin-producing *Escherichia coli* strains. *Front. Microbiol.* **2020**, *10*, No. 3093.

(10) Motlagh, A. M.; Bhattacharjee, A. S.; Goel, R. Microbiological study of bacteriophage induction in the presence of chemical stress factors in enhanced biological phosphorus removal (EBPR). *Water Res.* **2015**, *81*, 1−14.

(11) Zhang, J.; Lu, T.; Song, Y.; Rocha, U. N. D.; Liu, J.; Nikolausz, M.; Wei, Y.; Richnow, H. H. Viral communities contribute more to the lysis of antibiotic-resistant bacteria than the transduction of antibiotic resistance genes in anaerobic digestion revealed by metagenomics. *Environ. Sci. Technol.* **2024**, *58*, 2346−2359.

(12) Tang, X.; Fan, C.; Zeng, G.; Zhong, L.; Li, C.; Ren, X.; Song, B.; Liu, X. Phage-host interactions: The neglected part of biological wastewater treatment. *Water Res.* **2022**, *226*, No. 119183.

(13) Zhang, Q.; Zhou, H.; Jiang, P.; Wu, L.; Xiao, X. Silver nanoparticles facilitate phage-borne resistance gene transfer in planktonic and microplastic-attached bacteria. *J. Hazard. Mater.* **2024**, *469*, No. 133942.

(14) Zhang, Q.; Zhou, H.; Qiao, J.; Jiang, P.; Xiao, X. New insight into nanomaterial-mediated dissemination of phage-borne resistance genes: Roles of humic acid and illumination. *Chem. Eng. J.* **2024**, *486*, No. 150276.

(15) Li, K.; Chen, Z.; Hao, W.; Ye, Z. Differential inhibition of tire wear particles on sludge dewatering by aging modes. *J. Hazard. Mater.* **2024**, *480*, No. 136214.

(16) Sun, T.; Cai, S.; Zhang, X.; Wang, D.; Zhang, W. Leaching hazards of tire wear particles in hydrothermal treatment of sludge: Exploring molecular composition, transformation mechanism, and ecological effects of tire wear particle-derived compounds. *Water Res.* **2024**, *257*, No. 121669.

(17) Akdogan, Z.; Guven, B. Microplastics in the environment: A critical review of current understanding and identification of future research needs. *Environ. Pollut.* **2019**, *254*, No. 113011.

(18) Li, Z. M.; Kannan, K. Mass loading, removal, and emission of 1,3-diphenylguanidine, benzotriazole, benzothiazole, *N*-(1,3-dimethylbutyl)-*N*′-phenyl-*p*-phenylenediamine, and their derivatives in a wastewater treatment plant in New York State, USA. *ACS EST Water* **2024**, *4*, 2721−2730.

(19) Okoffo, E. D.; Tscharke, B. J.; O'Brien, J. W.; O'Brien, S.; Ribeiro, F.; Burrows, S. D.; Choi, P. M.; Wang, X.; Mueller, J. F.; Thomas, K. V. Release of plastics to Australian land from biosolids end-use. *Environ. Sci. Technol.* **2020**, *54*, 15132−15141.

(20) Ding, J.; Meng, F.; Chen, H.; Chen, Q.; Hu, A.; Yu, C.; Chen, L.; Lv, M. Leachable additives of tire particles explain the shift in microbial community composition and function in coastal sediments. *Environ. Sci. Technol.* **2022**, *56*, 12257−12266.

(21) Ding, R.; Ouyang, Z.; Zhang, X.; Dong, Y.; Guo, X.; Zhu, L. Biofilm-colonized versus virgin black microplastics to accelerate the photodegradation of tetracycline in aquatic environments: Analysis of underneath mechanisms. *Environ. Sci. Technol.* **2023**, *57*, 5714−5725.

(22) Zeb, A.; Liu, W.; Ali, N.; Shi, R.; Zhao, Y.; Wang, J.; Wang, Q.; Khan, S.; Baig, A. M.; Liu, J.; et al. Impact of pristine and aged tire wear particles on *Ipomoea aquatica* and rhizospheric microbial communities: Insights from a long-term exposure study. *Environ. Sci. Technol.* **2024**, *58*, 21143−21154.

(23) Zhang, P.; Tang, X.; Qin, N.; Shuai, Y.; Wang, J.; Wang, H.; Ouyang, Z.; Jia, H. Advanced understanding of the natural forces accelerating aging and release of black microplastics (tire wear particles) based on mechanism and toxicity analysis. *Water Res.* **2024**, *266*, No. 122409.

(24) Xu, J.-Y.; Ding, J.; Du, S.; Zhu, D. Tire particles and its leachates: Impact on antibiotic resistance genes in coastal sediments. *J. Hazard. Mater.* **2024**, *465*, No. 133333.

(25) Ding, J.; Lv, M.; Zhu, D.; Leifheit, E. F.; Chen, Q.; Wang, Y.; Chen, L.; Rillig, M. C.; Zhu, Y. Tire wear particles: An emerging threat to soil health. *Crit. Rev. Environ. Sci. Technol.* **2023**, *53*, 239−257.

(26) Huang, Q.; Wang, J.; Wang, J.; Yu, D.; Zhan, Y.; Liu, Z. Emerging health risks of crumb rubber: Inhalation of environmentally persistent free radicals via saliva during artificial turf activities. *Environ. Sci. Technol.* **2023**, *57*, 21005−21015.

(27) Liu, Z.; Sun, Y.; Wang, J.; Li, J.; Jia, H. In vitro assessment reveals the effects of environmentally persistent free radicals on the toxicity of photoaged tire wear particles. *Environ. Sci. Technol.* **2022**, *56*, 1664−1674.
(28) Xu, Q.; Li, G.; Fang, L.; Sun, Q.; Han, R.; Zhu, Z.; Zhu, Y. Enhanced formation of 6PPD-Q during the aging of tire wear particles in anaerobic flooded soils: The role of iron reduction and environmentally persistent free radicals. *Environ. Sci. Technol.* **2023**, *57*, 5978−5987.
(29) Zhao, H. N.; Hu, X.; Gonzalez, M.; Rideout, C. A.; Hobby, G. C.; Fisher, M. F.; McCormick, C. J.; Dodd, M. C.; Kim, K. E.; Tian, Z.; Kolodziej, E. P. Screening *p*-phenylenediamine antioxidants, their transformation products, and industrial chemical additives in crumb rubber and elastomeric consumer products. *Environ. Sci. Technol.* **2023**, *57*, 2779−2791.
(30) Ambros, C. L.; Ehrmann, M. A. Distribution, inducibility, and characterisation of prophages in *Latilactobacillus sakei*. *BMC Microbiol.* **2022**, *22*, No. 267.
(31) Sausset, R.; Krupova, Z.; Guédon, E.; Peron, S.; Grangier, A.; Petit, M.-A.; De Sordi, L.; De Paepe, M. Comparison of interferometric light microscopy with nanoparticle tracking analysis for the study of extracellular vesicles and bacteriophages. *J. Extracell. Biol.* **2023**, *2*, No. e75.
(32) Wang, K.-L.; Zhang, J.; Min, D.; Lv, J.; Liu, D.; Yu, H. Detection and quantification of antimicrobial-resistant cells in aquatic environments by bioorthogonal noncanonical amino acid tagging. *Environ. Sci. Technol.* **2022**, *56*, 15685−15694.
(33) Capolupo, M.; Sørensen, L.; Jayasena, K. D. R.; Booth, A. M.; Fabbri, E. Chemical composition and ecotoxicity of plastic and car tire rubber leachates to aquatic organisms. *Water Res.* **2020**, *169*, No. 115270.
(34) Ding, J.; Lv, M.; Wang, Q.; Zhu, D.; Chen, Q.; Li, X. Q.; Yu, C.; Xu, X.; Chen, L.; Zhu, Y. Brand-specific toxicity of tire tread particles helps identify the determinants of toxicity. *Environ. Sci. Technol.* **2023**, *57*, 11267−11278.
(35) Chen, L.; Liu, Z.; Yang, T.; Zhao, W.; Yao, Y.; Liu, P.; Jia, H. Photoaged tire wear particles leading to the oxidative damage on earthworms (*Eisenia fetida*) by disrupting the antioxidant defense system: The definitive role of environmental free radicals. *Environ. Sci. Technol.* **2024**, *58*, 4500−4509.
(36) Kim, G.; Lee, S. Characteristics of tire wear particles generated by a tire simulator under various driving conditions. *Environ. Sci. Technol.* **2018**, *52*, 12153−12161.
(37) Liu, S.; Liu, G.; Yang, L.; Li, D.; Zheng, M. Critical influences of metal compounds on the formation and stabilization of environmentally persistent free radicals. *Chem. Eng. J.* **2022**, *427*, No. 131666.
(38) Vejerano, E.; Lomnicki, S.; Dellinger, B. Formation and stabilization of combustion-generated environmentally persistent free radicals on an $Fe(III)_2O_3$/silica surface. *Environ. Sci. Technol.* **2011**, *45*, 589−594.
(39) Shao, B.; Mao, L.; Qu, N.; Wang, Y.; Gao, H.; Li, F.; Qin, L.; Shao, J.; Huang, C.; Xu, D.; Xie, L.; Shen, C.; Zhou, X.; Zhu, B. Mechanism of synergistic DNA damage induced by the hydroquinone metabolite of brominated phenolic environmental pollutants and Cu(II): Formation of DNA-Cu complex and site-specific production of hydroxyl radicals. *Free Radicals Biol. Med.* **2017**, *104*, 54−63.
(40) Truong, H.; Lomnicki, S.; Dellinger, B. Potential for misidentification of environmentally persistent free radicals as molecular pollutants in particulate matter. *Environ. Sci. Technol.* **2010**, *44*, 1933−1939.
(41) Dion, M. B.; Oechslin, F.; Moineau, S. Phage diversity, genomics and phylogeny. *Nat. Rev. Microbiol.* **2020**, *18*, 125−138.
(42) Silpe, J. E.; Duddy, O. P.; Bassler, B. L. Induction mechanisms and strategies underlying interprophage competition during polylysogeny. *PLoS Pathog.* **2023**, *19*, No. e1011363.
(43) Liu, H.; Li, H.; Qiu, L.; Xie, Q.; Lu, Y.; Chen, B.; Wang, H.; Long, Y.; Hu, L.; Fang, C. Alteration of the migration trajectory of antibiotic resistance genes by microplastics in a leachate activated sludge system. *Environ. Pollut.* **2023**, *333*, No. 121981.
(44) Antonelli, A.; D'Andrea, M. M.; Brenciani, A.; Galeotti, C. L.; Morroni, G.; Pollini, S.; Varaldo, P. E.; Rossolini, G. M. Characterization of *poxtA*, a novel phenicol-oxazolidinone-tetracycline resistance gene from an MRSA of clinical origin. *J. Antimicrob. Chemother.* **2018**, *73*, 1763−1769.
(45) Crowe-McAuliffe, C.; Murina, V.; Turnbull, K. J.; Huch, S.; Kasari, M.; Takada, H.; Nersisyan, L.; Sundsfjord, A.; Hegstad, K.; Atkinson, G. C.; Pelechano, V.; Wilson, D. N.; Hauryliuk, V. Structural basis for PoxtA-mediated resistance to phenicol and oxazolidinone antibiotics. *Nat. Commun.* **2022**, *13*, No. 1860.
(46) Prakash, R.; Garg, A.; Arya, R.; Kumawat, R. K. Chronicity of high and low level mupirocin resistance in *Staphylococcus aureus* from 30 Indian hospitals. *Sci. Rep.* **2023**, *13*, No. 10171.
(47) Wipf, J. R. K.; Perreten, V. Discovery of novel MLSB resistance methylase genes and their associated genetic elements in *Staphylococci*. *Curr. Clin. Microbiol. Rep.* **2016**, *3*, 42−52.
(48) Du Toit, A. Phages get snappy. *Nat. Rev. Microbiol.* **2024**, *22*, 324.
(49) Baker-Austin, C.; Wright, M. S.; Stepanauskas, R.; McArthur, J. V. Co-selection of antibiotic and metal resistance. *Trends Microbiol.* **2006**, *14*, 176−182.
(50) Maurya, A. P.; Rajkumari, J.; Bhattacharjee, A.; Pandey, P. Development, spread and persistence of antibiotic resistance genes (ARGs) in the soil microbiomes through co-selection. *Rev. Environ. Health* **2020**, *35*, 371−378.
(51) Ding, J.; Zhu, D.; Wang, H.; Lassen, S. B.; Chen, Q.; Li, G.; Lv, M.; Zhu, Y. Dysbiosis in the gut microbiota of soil fauna explains the toxicity of tire tread particles. *Environ. Sci. Technol.* **2020**, *54*, 7450−7460.
(52) Smolders, E.; Degryse, F. Fate and effect of zinc from tire debris in soil. *Environ. Sci. Technol.* **2002**, *36*, 3706−3710.
(53) De Wever, H.; Verachtert, H. Biodegradation and toxicity of benzothiazoles. *Water Res.* **1997**, *31*, 2673−2684.
(54) Hwang, C.; Choi, M. H.; Kim, H. E.; Jeong, S. H.; Park, J. U. Reactive oxygen species-generating hydrogel platform for enhanced antibacterial therapy. *NPG Asia Mater.* **2022**, *14*, No. 72.

https://doi.org/10.1021/acs.est.4c12499
Environ. Sci. Technol. 2025, 59, 11974−11984